ELSEVIER

Physica B 248 (1998) 387–394

PHYSICA B

Surface morphology by reflectivity of coherent X-rays

I.K. Robinson[a,*], J.A. Pitney[a], J.L. Libbert[a], I.A. Vartanyants[a,b]

[a] *Department of Physics, University of Illinois, Loomis Laboratory of Physics, 1110 West Green Street, Urbana, IL 61801, USA*
[b] *Institute of Crystallography, Moscow, Russian Federation, USA*

Abstract

Coherent X-ray diffraction (CXD) is a new technique made possible by the enhanced brilliance specifications of hard X-ray wigglers and undulators, especially at third-generation synchrotron radiation sources. CXD differs from conventional diffraction in that it uses a microscopic beam that is close to fully coherent one. The resulting diffraction pattern is related to the Fourier transform of the entire object illuminated by the beam, and hence is sensitive to any fluctuations within it, whether these are in space or in time. We have observed CXD effects in the near-specular reflectivity from silicon wafers. We introduce a simple theoretical formalism for explaining the origin of the coherent diffraction signal in a reflectivity experiment, in which we find a slow but distinct evolution of the pattern with the perpendicular component of momentum transfer, q_z. We demonstrate a practical energy dispersive method of measuring this q_z-dependence. © 1998 Published by Elsevier Science B.V.

Keywords: Coherent X-ray diffraction; Reflectivity; Morphology

The many ways that X-ray diffraction can be applied to the study of surface structure are summarised in the form of a roadmap of reciprocal space in Fig. 1. This figure was first presented at the second SXNS conference 6 years ago. The different regions of reciprocal space provide different kinds of information about the surface under examination. During the 6-year period leading up to the present SXNS-5 conference, the roadmap has not changed, but the focus of the conference has migrated towards the origin, and there has been considerable growth in interest in the region marked *non-specular reflectivity*. That region has strong overlap with neutron-based techniques, which are also represented in SXNS-5. It will be demonstrated in this paper that the *non-specular reflectivity* region also offers the greatest possibilities for the use of coherent X-ray beams to study surfaces.

In the context of the reflectivity region in Fig. 1, the words *surface structure* should be more specifically replaced by *surface morphology* to imply that the information available has limited resolution, and so the positions of individual atoms will not be accessible. The connection between morphology and the data attainable in a reflectivity experiment has been elaborated clearly in the 1988 paper of Sinha et al. [1]. There, the statistical properties of

* Corresponding author. Tel.: + 1 217 2442949; fax: 1 217 3336126; e-mail: ikr@uiuc.edu.

0921-4526/98/$19.00 © 1998 Published by Elsevier Science B.V.
PII: S0921-4526(98)00357-3

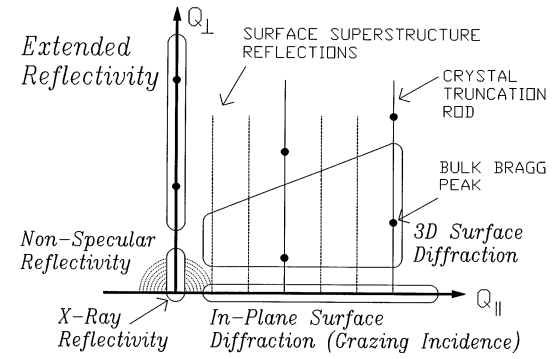

Fig. 1. Schematic map of reciprocal space indicating the names customarily given to different techniques that are sensitive to the surface. From Ref. [20].

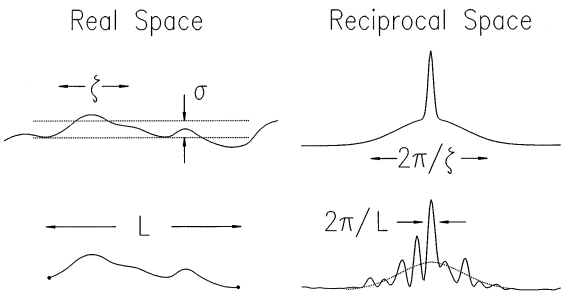

Fig. 2. Top: generic relationship between surface morphology in real space (left) and the reflectivity profile in reciprocal space (right). The real-space picture is of a surface height vs. lateral position; the reciprocal space picture is of intensity vs. lateral momentum transfer, such as would be measured by taking a rocking curve across the reflectivity. The broad component is the off-specular reflectivity referred to in Fig. 1. Bottom: equivalent situation when a coherent beam is used instead.

the surface under examination are summarised by a small number of parameters, an r.m.s. roughness, σ, an in-plane correlation length ζ, a fractal exponent and a distance cut-off parameter. The first two of these, and their connection to reciprocal space, are illustrated in the upper panels of Fig. 2.

The r.m.s. roughness σ in Fig. 2 must be defined with respect to some ideal reference plane. If there were not a well-defined reference plane, about which the surface is considered to fluctuate, there would not be a *specular* component to the diffraction from the surface at all. Conversely, the existence of this specular component, represented by the vertical line extending from the origin in Fig. 1 and as a sharp peak in the upper-right panel of Fig. 2, identifies the surface under investigation as having the property of possessing a reference plane. The fluctuations about the reference plane always return to the plane in the long range; if they did not, the surface would diverge in the long range and the specular diffraction component would vanish. The intensity of the specular component is given by the Fresnel reflectivity coefficient corresponding to the value of q_z, the perpendicular momentum transfer, modified by a Debye–Waller-like factor featuring the r.m.s. roughness, σ [1].

The in-plane correlation length ζ represents the lateral distance over which the fluctuations away from the reference plane take place. Points separated by distances which are small compared with ζ have essentially the same height while points separated by distances large compared with ζ have different heights. In reciprocal space this gives a diffuse component to the reflectivity profile which is the *non-specular reflectivity* region of Fig. 1. The characteristic width of the profile is given by the inverse of the in-plane correlation length ζ. The reason that a smooth distribution is obtained is that, associated with the diffraction process, there lies an implicit Fourier transform with a large range of spatial integration, which leads to an *ensemble averaging* of the many specific examples of morphology within this region.

We will now consider what happens to this non-specular reflectivity when a *coherent* illuminating X-ray beam is utilised instead.

Coherent X-ray diffraction is just a diffraction experiment carried out with a coherent beam, usually by cutting down a large incoherent beam to a size comparable with its lateral coherence length. Two types of coherence length with different characteristics are needed to describe the beam. In the simplest case, the transverse (or lateral) coherence length, ξ, is determined by the source size, w, by $\xi = \lambda D/w$ where D is the distance from the source to the defining aperture. The longitudinal coherence length, $\xi_{\|}$, is determined by the monochromator resolution as $\lambda(\Delta\lambda/\lambda)^{-1}$. For the NSLS wiggler source at beamline X25 and a broadband multilayer monochromator at $\lambda = 1.5\,\text{Å}$ we

would have

$\xi_{vert} = 23\,\mu m,$

$\xi_{hor} = 6\,\mu m,$

$\xi_{\|} = 0.008\,\mu m.$

A theoretical flux estimate can be made fairly readily because it turns out to be independent of the beamline design details. If we assume we can collect and utilise exactly one coherence volume of the dimensions stated above, the flux, F_0, depends only on the source brilliance, B, the wavelength, λ, and the monochromator bandpass, $\Delta\lambda/\lambda$, according to

$$F_0 = B\lambda^2(\Delta\lambda/\lambda). \quad (1)$$

The theoretical number at X25 is $B = 2 \times 10^{13}$ photons/s/(nm rad)^2 which gives for F_0 with multilayer optics (2% bandwidth) almost 10^{10} photons/s. In real experiments with a 5 μm circular aperture and a multilayer monochromator we have observed as much as 10^7 photons/s. When we are obliged, for reasons explained below, to use a Si(1 1 1) monochromator, we expect to lose two orders of magnitude in coherent flux, and this is roughly what is observed. Conversely, an example of a very powerful source for CXD is an X-ray undulator with its natural spectral width around 2% in λ which allows us to use no monochromator at all. A coherent flux approaching 10^9 photons/s has already been recorded in this way at ESRF. These are the typical incident fluxes we have to work with in designing our coherent surface diffraction experiments and it partly explains why it is mainly the reflectivity region of reciprocal space in Fig. 1 that has been explored to date.

For coherence to be preserved during the diffraction process, $\xi_{\|}$ must be greater than the maximum *path length difference* (PLD) among all possible rays traversing the sample. Noting that $\xi_{\|}$ is smaller than the penetration depth in many potential samples, this constraint may be hard to achieve. For a given sample, this would typically limit the usable range of scattering angles, and hence momentum transfer. Fortunately, in the case of reflectivity, the PLD happens to be independent of the penetration depth because of the destructive interference of the deeper layers with the surface contribution. At the specular condition, the PLD is identically zero, and in the non-specular reflectivity region it is still exceedingly small.

If a diffraction experiment is now carried out with a beam that is cut down to a size smaller than $\xi_{vert} \times \xi_{hor}$, all parts of the sample will be illuminated coherently, and the resulting intensity will be the square of their *amplitude sum*. This intensity therefore contains *phase information* about the relative positions of all the scattering 'grains'. In this way, we avoid the ensemble average normally associated with X-ray diffraction from disordered systems. Instead of a broadened diffraction pattern with a width that is inversely related to the average grain size, we will see an interference pattern containing all the phase information. By analogy with light scattering, this is called a *speckle pattern*. The phase sensitivity is the essential advantage of coherent X-ray diffraction (CXD) over conventional diffraction methods, and has now been demonstrated in a number of experiments, mainly making use of the high brightness of wiggler and undulator sources [2–5]. Because of its sensitivity to the specific arrangement of scattering matter, the technique is acutely sensitive to *fluctuations* in that configuration, as has also been demonstrated [6–9].

This leads us to the explanation of the lower panel of Fig. 2, which corresponds to the same reflectivity experiment as in the upper panel, but using a coherent beam. The first difference is that a *finite* length of sample is probed because of the (sharp-edged) aperture used to cut out a small enough beam to maintain its essential coherence. The second difference is that the smooth diffuse part of the reflectivity profile becomes structured into speckles, as shown. The speckles represent a finite-bounded Fourier-like summation over the illuminated length of the sample, as we will see below. It is important to note that there is *no specular component* clearly distinguishable from any of the other speckles; there is no longer a separation of specular and non-specular reflectivity. There are two ways to understand this result. Firstly, the illuminated sample is finite sized, so all diffraction from it, including the specular part, must be broadened to a characteristic width, which is the size of each of the speckles. The second explanation is that the reference plane, relative to which the roughness must be specified, is not well defined for

such a short length of sample, so there is uncertainty in its specular peak position.

We have assumed for simplicity that the size of the illuminated sample is larger than the in-plane correlation length ζ, so this latter quantity is still meaningful, although strictly not in the sense of it being an ensemble average over the whole surface. The role of the in-plane correlation length ζ is similar to the incoherent case in that it determines the extent of lateral momentum transfer over which speckles will occur. If we were to average together the calculated speckle patterns from a large number of different examples of surfaces with the same roughness σ and the same in-plane correlation length ζ, we would be calculating the same ensemble average that the incoherent experiment sees. The superimposed solid and dotted curves in Fig. 2 illustrate this feature.

The basic experimental set-up for CXD is very simple: a beamlime, monochromator (to select $\xi_{\|}$), aperture (to match $\xi_{\perp}$), a diffractometer and a detector. The detector must have sufficiently high resolution to resolve the inherent width of the features of the diffraction pattern, which are the same as the width of the direct beam, broadened by Fraunhofer diffraction in the defining source aperture. If the detector is a distance D_2 away from the source aperture of size d, this width will be $\lambda D_2/d$, typically about 20 μm. This resolution can be achieved with a direct-reading charge-coupled device (CCD) which has the advantage of parallel readout but slow time resolution. Alternatively, a second small aperture can be followed by a scintillation or solid-state detector, operating in pulse-counting mode for excellent time resolution. Most of the experiments carried out to date have used the simplest possible optical configuration: a flat double-multilayer monochromator or direct undulator radiation and a small pinhole just before the sample. More recently, we have found that better definition of the beam edges is important, and so we have developed a 'roller blade' slit design which allows us to control the finish of the blades with precision [10].

The diffraction signal measured from a sample under coherent illumination conditions is the magnitude squared of the scattering amplitude *without any ensemble averaging*. We simply observe the direct summation over all atoms in the beam,

$$A(\boldsymbol{q}) \propto \sum_j f \exp(i\boldsymbol{q}\cdot\boldsymbol{r}_j). \tag{2}$$

The surface is conveniently defined by a single-valued boundary function $z = h(x)$, where the z-direction is taken to be perpendicular to the surface, and x represents the two coordinates in the plane of the surface, $\boldsymbol{r} = (x, z)$ [1]. For simplicity, we are assuming a sample made up of a discrete lattice of a single kind of atoms with form factor, f. Eq. (2) can be rewritten by direct substitution [11] or equivalently in its integral form using Green's theorem [1].

$$A(\boldsymbol{q}) \propto F_{\mathrm{CTR}}(q_z) \sum_j \exp(iq_x x_j) \exp(iq_z h(x_j)), \tag{3}$$

where the summation has been reduced in dimension to a sum over *columns* of equally spaced atoms at lateral position x_j starting at height $h(x_j)$. The momentum transfer $\boldsymbol{q} = (q_x, q_z)$ has also been split into its components parallel to the surface, q_x (representing both components), and perpendicular, q_z. Apart from the starting-height factor, the sum in the z-direction is identical for all columns and takes the familiar form seen in the analysis of Crystal Truncation Rods (CTRs), which interpolates between the Bragg peaks in q_z [12],

$$F_{\mathrm{CTR}}(q_z) = f(1 - \exp(-iq_z a_3))^{-1}, \tag{4}$$

where a_3 is the vertical lattice spacing. If we were to continue the derivation for ordinary incoherent X-ray diffraction from surfaces, the next step would be to introduce some correlation function for $h(x)$, and take the ensemble average $\langle |A(\boldsymbol{q})|^2 \rangle$ [1,11]. Instead for CXD, we can look directly at $|A(\boldsymbol{q})|^2$, which should be compared directly with what is observed in the experiment.

The first factor in Eq. (3) is the well-known CTR amplitude, given in Eq. (4). This tells us that the signal is large near to Bragg peaks in q_z, and gets progressively smaller as we move away. CTRs are a standard feature of diffraction from surfaces and feature prominently in Fig. 1. Near to a bulk Bragg peak at G_z, the intensity falls off as $|(q_z - G_z)|^{-2}$. Importantly, since we are concerned with reflectivity, this is also true for the origin of reciprocal space, $G_z = 0$. The second factor in Eq. (3) can be

rewritten in the continuum limit as a kind of Fourier transform,

$$H(q_x, q_z) = \sum_j \exp(iq_x x_j)\exp(iq_z h(x_j)) = \int_{-d/2}^{d/2} \exp(iq_x x)\exp(iq_z h(x))\,\mathrm{d}x. \quad (5)$$

There are two unusual aspects of this Fourier transform compared with the familiar crystallographic expressions relating electron density in a structure with its diffraction pattern. The first is that the domain of the function is *finite*, cut off at the edges of the beam at positions $x = \pm d/2$. The second is that it is the Fourier transform in the x-direction of a *complex* argument with unit amplitude and a position-dependent phase, which depends on both the height function and the perpendicular momentum transfer: $e^{i\phi(x)}$, with $\phi(x) = q_z h(x)$.

In reflectivity experiments using a coherent beam at X25, we found behaviour which is consistent with this general formalism: a threshold was discovered in the q_z-dependence of coherent reflectivity from differently prepared Si(1 1 1) samples that was found to be in good correspondence with conventional profilometry measurements of roughness [13]. The expression in Eq. (5) is a more general version of the model that was also used in fitting static speckle from a GaAs/GaAlAs multilayer [4,5]. There, it was assumed that the coherent beam could be divided into 'blocks' that received different phases after diffracting from the discrete regions of the multilayer. The physical interpretation for $\phi(x)$ is clear: the X-ray beam incident on the sample at position x becomes phase shifted by an amount $\phi(x)$, which depends on height in the case of surface CXD, or, equivalently, the position of the diffracting planes in the case of multilayer, considered to be a coherent stack of internal surfaces. The *phase*-modulated beam undergoes mutual interference, which then results in the *amplitude* modulations seen in the speckle pattern.

The problem of inversion of Eq. (5) lies at the heart of the interpretation of static speckle. It is a more difficult problem than inversion of a diffraction pattern to obtain the electron density because the quantity sought is the phase. Inversion problems of this kind have been intensively studied in the past [14], and there are some powerful theoretical methods available. The most relevant analogy is to the problem of holographic reconstruction: transmission holography is achieved by coherent illumination of an transparent object over a finite aperture; the interference of all transmitted waves, recorded with sufficient resolution, is the hologram [15–17], which is closely related to the speckle pattern. If the object modulates the amplitude of the wave, this amplitude is the argument of the Helmholz–Kirchhoff integral that determines the hologram. But if the object has only phase contrast with no amplitude change, then the situation is identical to that of Eq. (5). For this reason, we have investigated the use of the iterative holographic reconstruction algorithm described in 1972 by Gerchberg and Saxton [18]. This has the potential to allow *reconstruction* of examples of surface morphology investigated with coherent X-ray reflectivity. We have made significant progress in this direction, with results reported in a poster at this conference and in Ref. [19].

It is instructive to consider the longitudinal coherence requirements mentioned above in the light of this theoretical understanding of the surface CXD. According to the formalism above, the path length difference (PLD) entering into the sum in Eq. (3) is just $\lambda\phi(x)$, which is very small indeed since the diffraction conditions (i.e. q_z) would be chosen to have $\phi(x)$ not changed by more than a few π. Large PLDs *are* present between the terms in Eq. (2), but these all accumulate in the factor F_{CTR}, which is common to all terms of Eq. (3). The PLD constraint in the specular direction can therefore be written as

$$\lambda q_z \Delta h(x) < \xi_{\|}, \quad (6)$$

where $\Delta h(x)$ is the *excursion* of the height, $h(x)$, over the range $-d/2 < x < d/2$. Even in the case where $\xi_{\|}$ is extremely short, say 50λ for a multilayer monochromator or a raw undulator beam, there will be broadening in q_z of $F_{\mathrm{CTR}}(q_z)$ in Eq. (4), but this is already a slow-varying function. This means that we can take advantage of the highest coherent flux estimates. Expression Eq. (6) is considerably more forgiving than the PLD constraints on bulk diffraction, where the large penetration depth can

be insurmountable. Note that we are not necessarily constrained to the small-angle case of $q_z \approx 0$ if the surface is sufficiently flat.

There is also a PLD constraint on the *parallel* component of momentum transfer, q_x, which may be more important in the non-specular reflectivity situation. If the sample is illuminated by a coherent beam of size d, an additional PLD will accumulate across the sample whenever q_x is non-zero, and the following condition must also be satisfied:

$$\lambda|q_x|d < \xi_{\|}. \tag{7}$$

The appearance of q_z in the expression for $\phi(x)$ provides us with an opportunity to acquire additional information that is specific to the surface CXD problem. If we can measure $H(\boldsymbol{q})$ at a number of different q_z values but all derived from the same $h(x)$, then we would have redundant information concerning the common $h(x)$ function sought, coupled to the phases $\phi(x)$ through different coefficients q_z. The additional information could then be used in a reconstruction procedure. This is illustrated in Fig. 3, where the full function $H(q_x, q_z)$ is plotted as a contour map. The observed speckle patterns are horizontal cuts across this diagram, and the smooth evolution as q_z is varied can be seen immediately. For example, if the speckle pattern is measured at a particular value of q_z, and the function $h(x)$ is somehow derived from it, then the pattern can be verified at other values of q_z as a validity check.

There is a practical difficulty with this method, which is the experimental problem of varying q_z without changing anything else, notably the position of the sample and its illuminated area. Angle-dispersive methods are simply out of the question since the typical sphere of confusion between the axes of an X-ray diffractometer is around 40 μm and the illuminated area must be kept constant within much less than 1 μm. Moreover, in the specular reflection geometry, changing q_z would require changing the incidence angle, and so changes the footprint size of the beam on the sample.

An elegant solution is to change q_z by changing the X-ray *energy* instead. In this way, the sample geometry and the positions of the beam-defining slits are not changed. On a bending magnet or wiggler beamline this would be achieved by scanning the monochromator. A slight disadvantage is that the beamline optics also introduces a phase structure in the incident beam (which distorts the resulting speckle), and this will change as the monochromator is moved. The method will work best with raw undulator beams, where the only adjustment is of the undulator gap. An excellent alternative is to use a white incident beam and an energy-sensitive detector, such as a cryogenic solid-state detector or PIN diode. With present technology, this would not be possible with position readout as well, but only in the single-channel mode behind an analyzing slit.

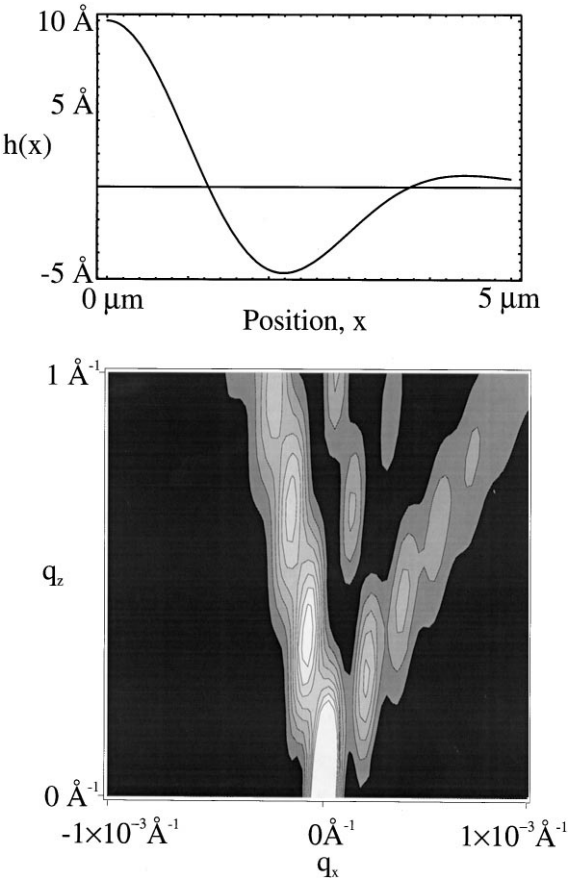

Fig. 3. Simulated speckle pattern from a one-dimensionally rough surface. Contours of $H(\boldsymbol{q})$ are plotted as a function of q_x and q_z. In general, there are two components to the in-plane momentum transfer q_x, which would make the diagram three dimensional. Note the extreme anisotropy between the scales of the q_x and the q_z axes.

We have made some preliminary measurements of surface coherent diffraction in this way, using the X25 wiggler, by scanning the multilayer monochromator. The data were collected at a fixed incidence and exit angle with a fixed aperture, thereby guaranteeing an immobile footprint on the sample. The sample was an epitaxial SiGe alloy film, which was rough due to instabilities occurring during its growth. The results in Fig. 4, show that the gross features of the coherent diffraction pattern are conserved, confirming that we were successful in controlling the footprint. The most noticeable feature is the apparent shrinking of the scale of the pattern at higher energy. This is because the horizontal axis measures the angular position of the exit beam; if the data had been plotted vs. q_x the shrinking effect would have been avoided. There are, nevertheless, perceptible differences in the fine structure between the data at different incident beam energies, which should provide information that is helpful in constraining the fitting of the data. Attempts at simultaneous fitting to a unique $h(x)$ function are still in progress at this time.

In conclusion, we have demonstrated that additional information about a surface can be obtained when a reflectivity experiment is carried out using a coherent beam instead of an incoherent one. For flux reasons, the method is practical at the present time for the specular and non-specular reflectivity regions which are sensitive to morphological (as opposed to atomic-scale) information about the surface under investigation. By developing a simple theoretical formalism for explaining the origin of the coherent diffraction signal in a reflectivity experiment, we see that there should be a slow but distinct evolution of the pattern with the perpendicular component of momentum transfer, q_z. Finally, we have demonstrated a practical energy dispersive method of measuring this q_z-dependence.

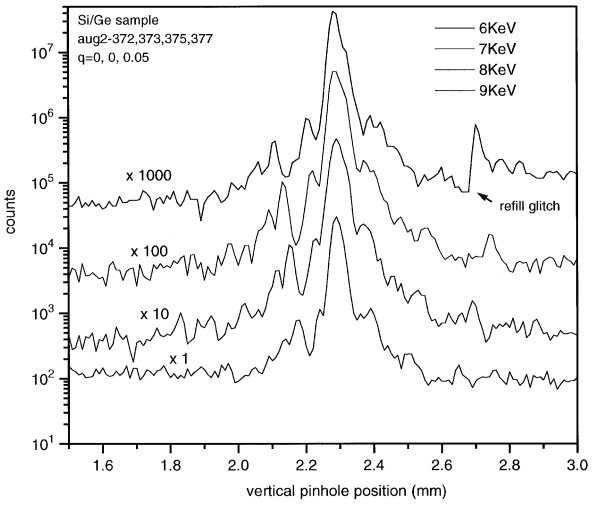

Fig. 4. Surface static CXD patterns measured in reflection from a SiGe sample at the X25 beamline at NSLS. Between the traces, only the identical beam energy was changed, as indicated. Clear similarities between the curves can be seen, but differences also. The systematic trends should be compared (qualitatively) with those of Fig. 3.

Acknowledgements

We are grateful for the assistance of L. Berman and Z. Yin at the X25 beamline of the NSLS. The NSLS is supported by the U.S. DOE under grant DE-AC012-76CH00016. The research was supported by the U.S. National Science Foundation under project number DMR93-15691.

References

[1] S.K. Sinha, E.B. Sirota, S. Garoff, H.B. Stanley, Phys. Rev. B 38 (1988) 2297.
[2] M. Sutton, S.G.J. Mochrie, T. Greytak, S.E. Nagler, L.E. Berman, G.A. Held, G.B. Stephenson, Nature 352 (1991) 608.
[3] Z.H. Cai, B. Lai, W.B. Yun, I. McNulty, K.G. Huang, T.P. Russell, Phys. Rev. Lett. 73 (1994) 82.
[4] I.K. Robinson, R. Pindak, R.M. Fleming, S.B. Dierker, K. Ploog, G. Grübel, D.L. Abernathy, J. Als-Nielsen, Phys. Rev. B 52 (1995) 9917.
[5] D.L. Abernathy, J. Als-Nielsen, S.B. Dierker, R.M. Fleming, G. Grübel, R. Pindak, K. Ploog, I.K. Robinson, Solid State Electron. 40 (1996) 531.
[6] S. Brauer, G.B. Stephenson, M. Sutton, R. Brüning, E. Dufresne, S.G.J. Mochrie, G. Grübel, J. Als-Nielsen, D.L. Abernathy, Phys. Rev. Lett. 74 (1995) 2010.
[7] S.B. Dierker, R. Pindak, R.M. Fleming, I.K. Robinson, L. Berman, Phys. Rev. Lett. 75 (1995) 449.
[8] T. Thurn-Albrecht, W. Steffen, A. Patkowski, G. Meier, E.W. Fischer, G. Grübel, D. Abernathy, Phys. Rev. Lett. 77 (1996) 5437.
[9] O.K.C. Tsui, S.G.J. Mochrie, to be published.
[10] J.L. Libbert, J.A. Pitney, I.K. Robinson, J. Synchrotron Rad. 4 (1997) 125.

[11] I.K. Robinson, E.H. Conrad, D.S. Reed, J. Phys. (France) 51 (1990) 103.
[12] I.K. Robinson, Phys. Rev. B. 33 (1986) 3830.
[13] J.L. Libbert, R. Pindak, S.B. Dierker, I.K. Robinson, Phys. Rev. B 56 (1997) 6454.
[14] G.W. Stroke, An Introduction to Coherent Optics and Holography, Academic Press, New York, 1966.
[15] D. Gabor, Nature 161 (1948) 777.
[16] M. Howells, C. Jacobsen, J. Kirz, R. Feder, K. McQuaid, S. Rothman, Science 238 (1987) 514.
[17] C. Jacobsen, M. Howells, J. Kirz, S. Rothman, J. Opt. Soc. Am. 7 (1990) 1847.
[18] R.W. Gerchberg, W.O. Saxton, Optik 35 (1972) 237.
[19] I.A. Vartanyants, J.A. Pitney, J.L. Libbert, I.K. Robinson, Phys. Rev. B 55 (1997) 13 193.
[20] I.K. Robinson, E. Vlieg, in: H. Zabel, I.K. Robinson (Eds.), Surface X-ray and Neutron Scattering, vol. 55, Springer, Berlin, 1992.